# Numerical 2D study of air flow controlled by passive technique in solar air collectors

Omar Mahfoud [1,2*], Merouane Zedayria [3], Abdelhafid Moummi [1] and Noureddine Moummi [1]

[1] Laboratoire de Génie Mécanique, Université Mohamed Khider,
B.P. 145, 07000, Biskra, Algeria

[2] Centre de Développement des Energies Renouvelables, CDER
[3] B.P. 62, Route de l'Observatoire, Bouzaréah 16430, Algiers, Algeria

Laboratoire d'Energétique Appliquée et de Pollution, LEAP
Université Mentouri, B.P. 325, 25000, Constantine, Algeria

**Abstract** - *The article presents a numerical simulation on air flow and heat transfer characteristics in solar air collectors mounted with obstacles. Computational Fluid Dynamics, 'CFD' based on the finite volume method, SIMPLE algorithm and the turbulence standard (k - ε) model have been implemented. A numerical 2D model of dynamic air vein solar collectors with 1400 mm length and 25 mm air gap was used to evaluate hydrodynamic and heat transfer phenomena of flow patterns in the annular passageways, precisely the heat transfer around 13 chicanes. The chicane is formed with two parts: the first is perpendicular to the air flow and the second is titled (α = 60°), they are mounted in successive rows, oriented perpendicular to the air flow. It is apparent that the turbulence created by the chicanes resulting in greater increase in heat transfer over the air vein. The pressure drops are analyzed vs. the Reynolds number and shown good agreements with experimental and semi-empirical relationship results. The mass flow rates effect on the velocity magnitude is analyzed. It was found that the mass flow rate variation has a slight effect on velocity evolution.*

**Résumé** – *L'article présente une simulation numérique de l'écoulement de l'air et les caractéristiques d'échange thermique à l'intérieur des capteurs solaires à air munis avec des obstacles. La technique de la simulation CFD basé sur la méthode des volumes finis a été mise en œuvre avec l'algorithme SIMPLE et le modèle de turbulence standard (k - ε). Un modèle numérique en 2D de la veine d'air mobile avec une longueur de 1400 mm et une hauteur de 25 mm a été utilisé pour évaluer les phénomènes de transfert de chaleur hydrodynamiques et la configuration de l'écoulement dans la veine d'air mobile et autour de 13 chicanes. La chicane est formée de deux parties: la première est perpendiculaire à l'écoulement de l'air et la deuxième est inclinée (α = 60 °). Elles ont été montées en rangées orientées perpendiculairement à l'écoulement de l'air. Il est évident que la turbulence créée par les chicanes résultant en une grande augmentation du transfert de chaleur le long de la veine d'air. Les pertes de charge sont analysées par rapport au nombre de Reynolds et montre un bon accord avec les résultats expérimentaux, ainsi que les relations semi-empiriques. L'analyse de la variation du débit a montré un faible effet sur l'évolution de la vitesse magnitude.*

**Mots clés**: Capteur solaire à air - Chicanes - Transfert de chaleur - Contrôle de l'écoulement - CFD.

---

* omarconj@yahoo.fr , o.mahfoud@cder.dz

# 1. INTRODUCTION

Solar air collector major problem is the low heat exchanges made with air in the dynamic air vein. These exchanges do not provide better performance and improved thermal efficiency of these systems.

The improved performance of the solar collectors was to limit heat loss from the absorber and the ambiance with a judicious choice of the collector components. Recently, performance optimization focused on the air circulation. Many types of solar air collectors have been constructed and tested over the world, with the main objective to collect maximum solar energy with a minimum cost. To achieve this goal, major works are now explored.

The first work on the numerical investigation of flow and heat transfer characteristics in a duct with the concept of periodically fully developed flow was introduced by Patankar *et al.* 1977.

To make the solar air heaters economically viable, their thermal efficiency needs to be improved by enhancing the heat transfer coefficient, which can be achieved by creating a fully turbulent flow in these systems and minimizing the heat loss with appropriate pressure drop and other factors. There are different factors have been developed in literatures (Dipprey *et al.* 1963, Hollands *et al.* 1981, Choudhury *et al.* 1991, Hachemi 1995, Youcef-Ali 2005, Moummi *et al.* 2004).

In order to enhance rate of heat transfer to flowing air in the collectors' air vein and in heat exchanger various surface roughness and turbulence generators viz, ribs, baffles and delta winglets are considered as an effective technique. In the solar air heater vein, presence of laminar sub-layer between the absorber plate and flowing air is generally considered to be the main cause of thermal resistance for heat transfer. Artificially roughened absorber plate is considered to be a good methodology to break laminar sub-layer in order to reduce thermal resistance and to increase heat transfer coefficient, Prasard *et al.* 1998.

Literature on application of artificial roughness in a solar air heater covers wide range of roughness geometries for studying heat transfer and friction characteristics. General arrangement of different types of roughness geometries reported by various investigators, they studied heat transfer enhancement and friction loss by fixing protruding wires of different shapes, size and orientations as an artificial roughness element on absorber plate as in (Prasad *et al.* 1998, Sahu *et al.* 2005, Gupta *et al.* 1997, Karwa *et al.* 1999, Saini *et al.* 1997, 2008, Karmare *et al.* 2007). Based on these literatures reviews following, it has been found that roughness geometries being used in solar air heaters are of many types depending upon shapes, size, arrangement and orientations of roughness elements on the absorber plate.

The heat transfer augmentation in solar air collectors with artificial roughness is accompanied by a substantial increase in pressure drops, Chouchane *et al.* 2009. An ideal design must involve a balance between friction losses and heat transfer rates and thus the designer must decide how to tradeoff between these two factors. Nevertheless, the requirement for detailed and accurate measurement of the design parameters (temperature, pressure and velocity fields) is very difficult to be achieved, because the flow passages in compact heat exchangers are complex in geometry and of relatively small dimensions, Kanaris *et al.* 2005. The rapid development of computational tools permits the prediction of flow characteristics using CFD code simulation which is considered an effective tool to estimate momentum and heat transfer rates in this type of process equipment. Consequently, as CFD is more widely used in engineering design, it

is becoming of essential importance to know how reliably the flow features and the hydrothermal behavior can be reproduced in such air veins.

Literature reviews shows that there has been less attention to the dynamic and the hydrodynamics flow behavior around artificial roughness modeling by means of CFD.

The objective of this work is to study hydrodynamic and thermal behavior air flow around artificial roughness and the inlet mass flow rates effect on the flow structure and heat transfer degree of the thermal transfer in the case of air vein solar collectors. 2D CFD simulation model is investigated for different Reynolds number range.

## 2. FLOW CONFIGURATION AND MATHEMATICAL FOUNDATION

### 2.1 Chicane geometry and arrangement

Based on solar air flat plate collector usually used at the Mechanical Engineering Research Laboratory 'LGM' at Biskra University. The physical model investigated in this work is presented in Fig. 1a. The system of interest is horizontal square channel (dynamic air vein) with 13 chicanes placed on the bottom channel walls in successive rows arrangements as shown in Fig. 1a.

In the flow module, the air enters the vein at the inlet temperature, $T_i = 300\,K$ and flows over obstacles where $h_1$, $h_2$, e and b b are the obstacle orthogonal height, tilted ($\alpha = 60°$) part height, full chicane height and thickness, respectively with: $h_1 = 10\,mm$, $h_2 = 15\,mm$, $e = 17.5\,mm$ and $b = 0.4\,mm$ while the thin obstacle is set to $e / D_h = 0.35$. The vein height, H is 25 mm. The hydraulic diameter is $D_h \approx 2H$. The axial pitch or spacing between the chicanes is set to $p = 100\,mm$ in which $p / D_h = 2$ is defined as the chicanes pitch ratio.

### 2.2 Mathematical Modeling

To build numerical models sufficiently detailed and accurate, it must sometimes take account of some assumptions. For this, we imply:
- Two-dimensional steady-state flow with heat transfer.
- Flow fully developed, turbulent and incompressible.
- Constant fluid properties.
- Body forces, viscous dissipation and radiation heat transfer are ignored.

Following the introduction of the above assumptions, the Reynolds Averaged Navier–Stokes (RANS) equations and the energy equations govern the transport of the averaged flow quantities in the air vein collector, Fluent help 2006. They can be written in Cartesian tensor form as:

Continuity equation-

$$\frac{\partial}{\partial x_i}(u_i) = 0 \tag{1}$$

Momentum equation-

$$\frac{\partial}{\partial x_j}(u_i u_j) = -\frac{1}{\rho}\frac{\partial P}{\partial x_j} + \frac{\partial}{\partial x_j}\left[\frac{\mu}{\rho}\left(\frac{\partial u_i}{\partial x_j} - \rho\overline{u_i' u_j'}\right)\right] \tag{2}$$

The variable $\rho$ is the fluid density, and $u_i$ is a mean component of velocity in the direction $x_i$, $\mu$ is the dynamic viscosity, $P$ is the pressure, and $u'$ is a fluctuating component of velocity. Repeated indices indicate summation from one to two by assuming tow-dimensional problems.

Energy equation-

$$\frac{\partial}{\partial x_j}(u_i \times T) = \frac{\partial}{\partial x_i}\left(a\frac{\partial T}{\partial x_j}\right)\tag{3}$$

where $a$ is given by: $a = \lambda/\rho \times C_p$

The Reynolds-averaged approach to turbulence modeling requires that the Reynolds stresses, $-\rho \times \overline{u_i' u_j'}$ must be modeled in order to close the equation (2), Fluent 2006, Launder *et al.* 1972. In this paper, the Boussinesq hypothesis are employed to relate the Reynolds stresses to the mean velocity gradients with the same shape as a viscid stress tensor, i.e. that the turbulent flow behaves as a fluid of viscosity $\mu_t$ as seen in the equation below:

$$-\rho \times \overline{u_i' u_j'} = \mu_t \times \left(\frac{\partial u_i}{\partial x_j} + \frac{\partial u_j}{\partial x_i}\right) - \frac{2}{3}\rho \times k \times \delta_{ij}\tag{4}$$

where $k$ is the turbulent kinetic energy as defined $k = \frac{1}{2}\overline{u_i' u_i'}$ and $\delta_{ij}$ is the Kronecker delta. An advantage of Boussinesq approach is the relatively low computational cost associated with the computation of the turbulent viscosity; $\mu_t$ depends on the close equation models. In Fluent, the Standard $(k-\varepsilon)$ model is the most widely used because of its robustness and is therefore valid only for fully turbulent flows, precision and relatively its low cost in computation time. This model is an example of two-equation models; turbulent kinetic energy and dissipation rate are obtained from the following equations.

$$\frac{\partial}{\partial x_i}(\rho \times k \times u_i) = \frac{\partial}{\partial x_j}\left[\left(\mu + \frac{\mu_t}{\sigma_k}\right) \times \frac{\partial k}{\partial x_j}\right] + G_k + G_b - \rho \times \varepsilon\tag{5}$$

$$\frac{\partial}{\partial x_i}(\rho \times \varepsilon \times u_i) = \frac{\partial}{\partial x_j}\left[\left(\mu + \frac{\mu_t}{\sigma_\varepsilon}\right) \times \frac{\partial \varepsilon}{\partial x_j}\right] + C_{\varepsilon 1}\frac{\varepsilon}{k} \times (G_k + C_{\varepsilon 2}G_b) - C_{\varepsilon 2} \times \rho \times \frac{\varepsilon^2}{k}\tag{6}$$

The term $G_k$, representing the production of the turbulence kinetic energy due to the average velocity gradient. From the exact equation for the transport of $k$, this term may be defined as:

$$G_k = -\overline{u_i' u_i'} \times \frac{\partial u_j}{\partial x_i}\tag{7}$$

To evaluate $G_k$ in a manner consistent with Boussinesq hypothesis;

$$G_k = \mu_t \times S^2\tag{8}$$

With $S = \sqrt{2 S_{ij} \times S_{ij}}$ where $S$ is the modulus of mean rate-of-strain tensor:

$$S_{ij} = \frac{1}{2} \times \left\{ \frac{\partial u_i}{\partial x_j} + \frac{\partial u_j}{\partial x_i} \right\}$$

And $G_b$ is the generation of the turbulence kinetic energy due to the buoyancy.

In the above equations, $C_{\varepsilon 1}$, $C_{\varepsilon 2}$ and $C_{\varepsilon 3}$ are constants. $\sigma_k$ and $\sigma_\varepsilon$ are the turbulent Prandtl numbers for k and $\varepsilon$, respectively. The effective viscosity $\mu_t$ is written by;

$$\mu_t = \rho \times C_\mu \times k^2 / \varepsilon \tag{9}$$

The model constants have the following values: $C_{\varepsilon 1} = 1.44$; $C_{\varepsilon 2} = 1.92$; $C_\mu = 0.09$; $\sigma_k = 1.0$; $\sigma_\varepsilon = 1.3$.

# 3. CFD MODELING, COMPUTATIONS AND VALIDATION

In order to investigate the solar air collector's performances, computational fluid dynamics (CFD) techniques allows us to build a numerical model to obtain more information inside flow field development and temperature distribution in rectangular space between two plates(dynamic air vein). The bottom plate is considered as adiabatic and topped with chicanes, by against the upper one considered as absorber that generates heat flux unless the other walls are assumed adiabatic.

In the present work, through the CFD modeling 66 computational blocks were created in order to describe accurately the collector geometry together with chicanes tilted parts, as presented in Fig. 1b. The grid mesh must meet specific requirements in terms of mesh size and type, Mahfoud *et al.* 2012. Special attention was given to the tilted and the orthogonal parts then to the near areas where increased variations of flow quantities are expected, so as to ensure a smooth convergence and to capture properly all fluid flow phenomena, as shown in Fig. 1. Thereafter, the modeling requires a choice of different settings of the computer code. The right adjustments made, the simulation was launched.
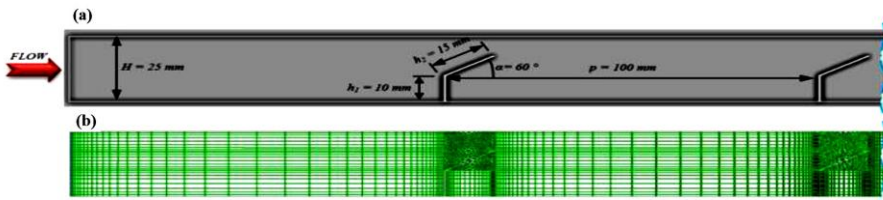


Fig. 1: Geometry of the CFD model; (a) Chicane dimensions (b) Grid

## 3.1 Geometrical aspect and grid independence

As part of this numerical approach, a grid independence procedure was implemented over grids with different numbers of cells, 14000 to 130000 cells. It is found that the variation of; surface heat transfer coefficient ($h_s$) and skin friction coefficient ($f$) are marginal when moving from 65300 to 130000 cells. Hence, there is no such advantage in increasing the cells number beyond this value. The grid system was adopted with non-uniform Cartesian grid and multi blocks. To considering convergent time and

solution precision, structured mesh was applied in major of blocks and unstructured in the rest. The mesh is refined at the regions with high gradients of temperature and velocity, which is near the vein inlet and around chicanes. Above these conditions, the grid system of 65300 cells was adopted for the current computational model, (Fig. 2).
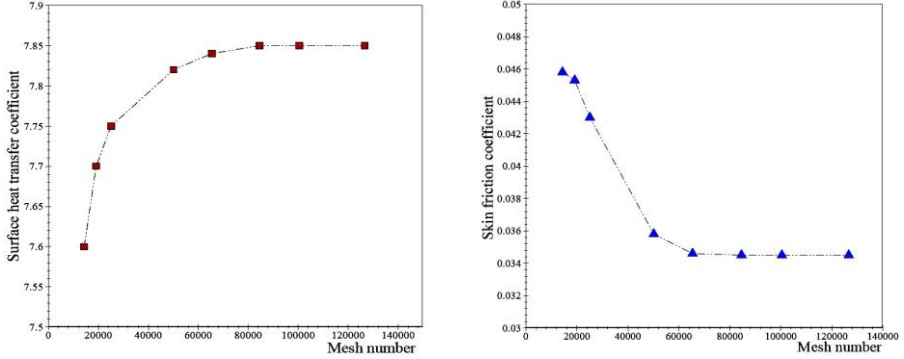


Fig. 2: Grid independence test

## 3.2 Post - processing

Once geometry is created and boundary conditions are defined, the mesh was exported to perform operations via CFD Fluent software. Based on finite volumes methods the main equations are solved using second order scheme for pressure and velocity. The coupled pressure-velocity refers to the numerical algorithm SIMPLE that uses combination between continuity and momentum equations to derive pressure equation. These steps are repeated with a precision of 1/1000.

The simulations first steps are to define the solver and models to apply. For temporary buoyancy driven flows, pressure based solver with energy equation model is considered appropriately. As the main focus is to be on transient solution, time is considered to be steady. Also, the $2^{nd}$ order implicit time formulation and Green-Gauss Cell Based are chosen rather than the first order as it improves the accuracy of the solution. All other inputs are left as the standards. The materials properties that are used are summarized in **Table 1**. Fluent 2006.

**Table 1**: Thermo physical properties

| Properties | Material | |
|---|---|---|
| | Air | Aluminium |
| Density, $\rho$, kg/m$^3$ | 1.225 | 2719 |
| Specific heat, $C_p$, J/kg.K | 1006.43 | 502.48 |
| Thermal conductivity, $\kappa$, W/m.K | 0.0242 | 202.4 |
| Viscosity, $\nu$, kg/m.s | $1.7894 \times 10^{-5}$ | |

## 3.3 Boundary conditions and validation

For a full length domain, uniform air mass flow rate is introduced at the inlet while a pressure outlet condition is applied at the exit. Constant air mass flow rate with 300 K ( Pr = 0.74) is assumed in the flow direction. The physical properties of the air have been assumed to remain constant at mean bulk temperature. Impermeable boundary and

no-slip wall conditions have been implemented over the channel walls. The constant flux of 482 W/m$^2$ was given at absorber wall while opposite side kept at adiabatic wall condition. The constant 300 K temperature condition is employed for chicanes as same the initial air temperature.

The results presented on Fig. 3, show the Reynolds number variation effect on the pressure drops between the dynamic air vein inlet and outlet. It's clear that are in good agreement with Simi-empirical relationship results as in Chouchane *et al.* 2009 and Youcef-Ali 2005 experimental results. It is seen that at laminar flow (Re < 2100), the pressure losses vary gradually in the range of (1 to 20 Pa), therefore the turbulent flow (Re > 2100), the difference is more significant (20 to 60 Pa).



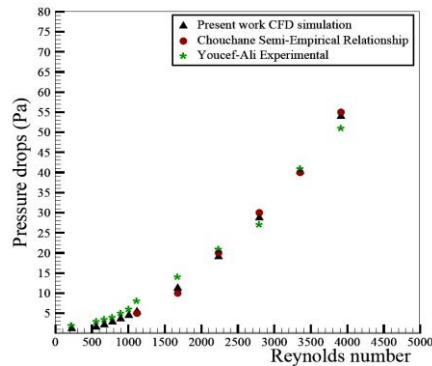Fig. 3: Pressure drops vs Reynolds number 100 < Re < 4500

## 4. RESULTS AND DISCUSSION

In a transient two-dimensional numerical simulation, once the numerical solutions have been obtained, there is considerable amount of data to be analyzed.

Qualitative results can be post-processed using commercial visualization software.

### 4.1 Hydrodynamic aspects

In order to highlight the chicanes influence on the air flow along the vein bottom wall. The direct observation through contours visualization appears as very practical guide to highlight hydrodynamic fluctuations characteristics.

### 4.1.1 Path lines contours

Typical path lines colored by radial velocity fields are shown in Fig. 4 b- and c-, when the inlet air flow mass has a value of $\dot{m} = 0.02 \text{ kg/s}$. The lowest values of the radial velocity of air shall be those adjacent to the downstream and upstream of the orthogonal chicanes parts, against on the tilted upper parts the high radial velocity values were recorded. This means that chicanes tilted parts increase velocity values at the passageway between absorber and chicanes. The converging passageway shape has a crucial role in the velocity evolution, so hydrodynamic instabilities are present and made by pairing and recirculation flow. The appearance of two secondary vortices exactly located at chicanes base on upstream and downstream. In addition, at chicane downstream two other vortices are seen as primary contra-rotary vortices, the greater

one which feeds adjacent vortex and it is observed that velocity high values are above the trailing edge, Fig. 4 c-.
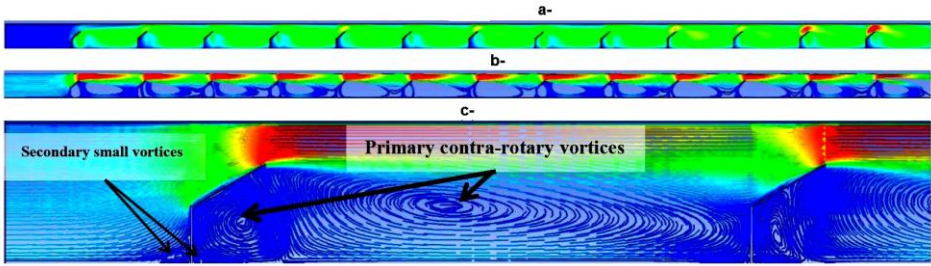


Fig. 4: a- Turbulence intensity, b- Radial velocity fields vectors, c- Path lines

## 4.2 Thermal aspects
### 4.2.1 Static temperature contours

Fig. 5 shows that the vortex structures generated by obstacles (chicanes) influence significantly on temperature field, so these obstacles induce more turbulence which means better air mixing and it will stimulate heat transfer as noted by Aoues *et al.* 2011, Mahboub *et al.* 2012. In the present work, it is observed that the air temperature increasing along the dynamic air vein length, where it reaches the value of 349 K, because the heated main flow moves along the chicanes due to upper parts inclinations and the secondary flow is trapped between two chicanes and the main flow where is powered with a brewing phenomenon which provokes a heat transfer from the hot flow to the cold one, therefore the chicanes provide a delaying aspect for more time for the heat transfer possesses which is confirmed by Moummi *et al.* 2010.
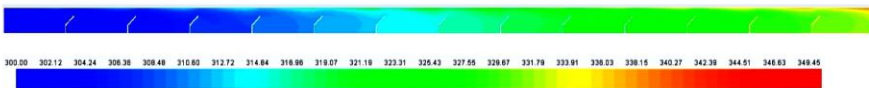


Fig. 5 Static temperature contours

## 4.3 Qualitative aspects

Different parameters profiles are plotted such as the velocity magnitude in several abscissas sections along the dynamic air vein, (Fig. 6).
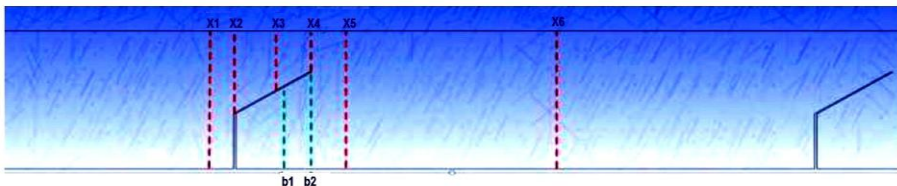


Fig. 6: Cross sections positions relative to the chicanes

### 4.3.1 Effect of air mass flow rates

Fig. 7, shows the velocity magnitude evolution across the vein height, just on the downstream and upstream of the chicanes obtained from CFD analysis. The velocity magnitude profiles are plotted in several abscissas sections on the axial positions;

$X1 = 0.08$ m; $X2 = 0.1$ m; $X3 = 0.107$ m; $X4 = 0.1134$ m; $X5 = 0.1154$ m; $X6 = 0.15$ m; $b1 = 0.1072$ m; $b2 = 0.1134$ m. $X1$ $X2$ $X3$ $X4$ $X5$ $X1$ $X1$ $b1$ , $b2$
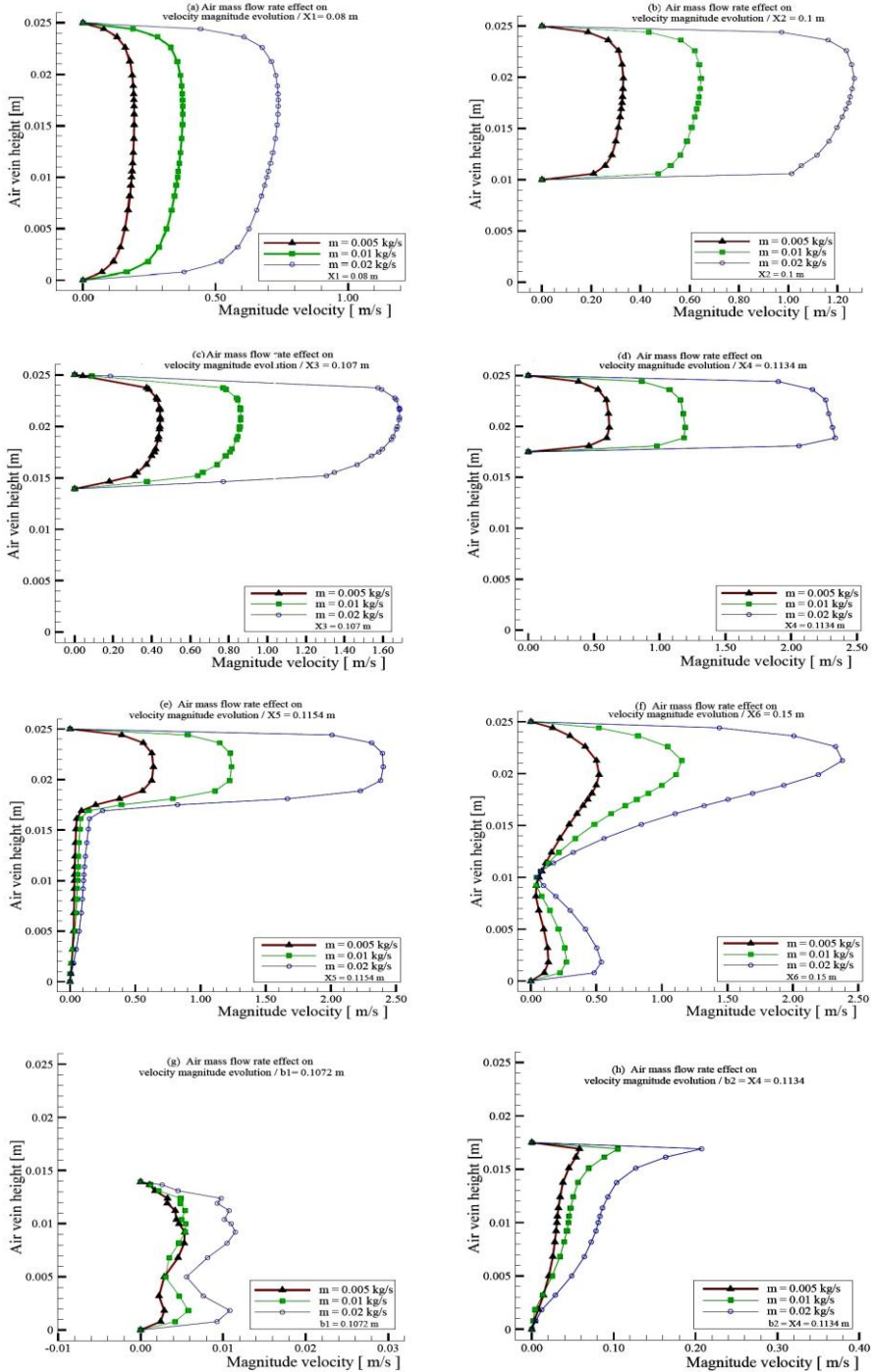
Fig. 7: Mass flow rates effect on the magnitude
velocity evolution at different axial locations

At $X1$ position, the parabolic profile is observed without any deformation when the air mass flow rate grows from 0.005 kg/s to 0.02 kg/s, this appearance maintains at positions $X2$, $X3$, $X4$ where the air flows on the chicane tilted part, except an increasing of the velocity magnitude value which is observed at $X4$ position and reached 0.60 m/s for low air mass flow rate value (0.005 kg/s) and the maximum value of 2.5 m/s is obtained for 0.02 kg/s.

At $X5$ position just downstream of the chicane, velocity profile changes appearance compared to $X1$ position and becomes almost nil at chicane height of (0.017 m), on the other hand the profile keeps the same shape on this section with same values compared to $X4$.

The air flow velocity profile at position $X6$, which at mid-distance between two chicanes is significantly disrupted and loses its parabolic shape due to the recirculation zone with slight perturbation at down. It is very important to note that the velocity magnitude becomes equal to zero value at orthogonal chicane part height (0.01 m).

The positions ($b1$, $b2$) located downstream and below the chicane tilted part, at these locations the velocity magnitude is slightly disturbed and keeps very minimal.

# 5. CONCLUSION

In this work, the hydrodynamic and heat transfer process in air solar collectors having roughened plate provided with artificial roughness (chicanes) with tilted parts has been made to carry out numerically as an illustrative example of the two-dimensional use in CFD. The work presents the methodology followed by the problem definition, the assumption of a mathematical model, its conversion into a numerical model, and the analysis of the obtained numerical solutions which has a good agreement with literatures.

The flow contours analysis show that the flow patterns in the dynamic air vein collectors were characterized by different regions and hydrodynamic instabilities are present and made by pairing and recirculation flow. The appearance of primary and secondary vortices just on upstream and downstream chicanes.

The vortex structures generated by obstacles (chicanes) involve better air mixing and it will stimulate heat transfer by convection, so increase significantly the outlet temperature.

The pressure drops are more and more important when the Reynolds number increase ($100 < \text{Re} < 4500$), the results shown good agreements with experimental results of Youcef-Ali, 2005 and semi-empirical relationship in Chouchane *et al.* 2009. The magnitude velocity is significantly influenced by increasing air mass flow rates from 0.005 kg/s to 0.02 kg/s.

# ACKNOWLEDGMENTS

# NOMENCLATURE

| | |
|---|---|
| L : air vein collector length, m | $\dot{m}$ : Air mass flow rate, kg/s |
| H : Air vein collector height, m | Pr : Prandtl number |
| $D_h$ : Hydraulic diameter, m | Re : Reynolds number |

| | |
|---|---|
| b : Full chicane height, m | Nu : Nusselt number |
| e : Chicane thickness, m | $\alpha$ : Chicane tilt, ° |
| $h_1$ : Chicane orthogonal part height, m | $\rho$ : Air density, kg/m$^3$ |
| $h_2$ : Chicane tilted part height, m | $C_p$ : Specific heat, J/kg.K |
| p : Axial pitch, m | $\kappa$ : Thermal conductivity, W/m.K |
| $T_i$ : Inlet temperature, K | $\nu$ : Viscosity, kg/m.s |

# REFERENCES

[1]  S. Youcef-Ali, '*Study and Optimization of the Thermal Performances of the Offset Rectangular Plate Fin Absorber Plates, with Various Glazing*', Renewable Energy, Vol. 30, N°2, pp. 271 – 280, 2005.

[2] K. Aoues, N. Moummi, M. Zellouf and A. Benchabane, '*Thermal Performance Improvement of Solar Air Flat Plate Collector: A Theoretical Analysis and an Experimental Study in Biskra, Algeria*', International Journal of Ambient Energy, Vol. 32, N°2, pp. 95 – 102, 2011.

[3] N. Chouchane, A. Moummi, B. Achour et N. Moummi, '*Modèles Empiriques de Calcul des Pertes de Charge dans un Conduit Rectangulaire Muni de Rugosités Artificielles - Cas des Insolateurs à Air*', Revue des Energies Renouvelables, Vol. 12 N°3, pp. 385 - 394, 2009..

[4] C. Choudhury and H.P. Garg, '*Design Analysis of Corrugated and Flat Plate Solar Air Heaters*', Renewable Energy, Vol. 1, N°5-6, pp. 595 – 607, 1991.

[5] D.P. Dipprey and R.H. Sabersky, '*Heat and Momentum Transfer in Smooth and Rough Tubes at Various Prandtl Numbers*', International Journal of Heat and Mass Transfer, Vol. 6, N°5, pp. 329 – 332, IN1, 333 - 353, 1963.

[6] Fluent, Help Documentations Inc., 2006.

[7] D. Gupta, S. Solanki and J.S. Saini, '*Thermohydraulic Performance of Solar Air Heaters with Roughened Absorber Plates*', Solar Energy, Vol. 61, N°1, pp. 33 – 42, 1997.

[8]  A. Hachemi, '*Thermal Performance Enhancement of Solar Air Heaters, by Fan-Blown Absorber Plate with Rectangular Fins*', International Journal of Energy Research, Vol. 19, N°7, pp. 567 – 578, 1995.

[9] K.G.T. Hollands and E.C. Shewan, '*Optimization of Flow Passage Geometry for Air-Heating Plate-Type Solar Collectors*', Transactions of ASME, Journal of Solar Energy Engineering, Vol. 103, pp. 323 – 330, 1981.

[10] A.G. Kanaris, A.A. Mouza and S.V. Paras, '*Flow and Heat Transfer in Narrow Channels with Corrugated Walls a CFD Code Application*', Chemical Engineering Research and Design, Vol. 83, N°5, pp. 460 – 468, 2005.

[11] S.V. Karmare and A.N. Tikekar, '*Heat Transfer And Friction Factor Correlation for Artificially Roughened Duct with Metal Grit Ribs*', International Journal of Heat and Mass Transfer, Vol. 50, N°21-22, pp. 4342 – 4351, 2007.

[12] R. Karwa, S.C.J. Solanki and S. Saini, '*Heat Transfer Coefficient and Friction Factor Correlation for the Transitional Flow Regime in Rib-Roughened Rectangular Ducts*', International Journal of Heat and Mass Transfer, Vol. 42, N°9, pp. 1597 – 1615, 1999.

[13] B.E. Launder and D.B. Spalding, '*Lectures in Mathematical Models of Turbulence*', Academic Press, England, 1972.

[14] C. Mahboub and N. Moummi, '*Calculation of the Glass Cover Temperature and the Top Heatloss Coefficient for 60° vee Corrugated Solar Collectors with Single Glazing*', Solar Energy, Vol. 86, N°2, pp. 804 – 808, 2012.

[15] O. Mahfoud, H. Oualli, M. Lebbi, S. Hanchi et A. Bouabdellah, '*Contrôle de l'Ecoulement de Taylor-Couette par l'Effet de la Déformation Radiale du Cylindre Intérieur*', Congrès Algérien de Mécanique, CAM Biskra, Algérie 16-17 Octobre, 2009.

[16] N. Moummi, S. Youcef-Ali, A. Moummi and J.Y. Desmons, '*Energy analysis of a solar air collector with rows of fins*', Renewable Energy, Vol. 29, N°13, pp. 2053 – 2064, 2004.

[17] N. Moummi, A. Moummi, K. Aoues, C. Mahboub and S. Youcef-Ali, '*Systematic Forecasts of Solar Collector's Performance in Various Sites of Different Climates in Algeria*', International Journal of Sustainable Energy, Vol. 29, N°3, pp. 142 – 150, 2010.

[18] S.V. Patankar, C.H. Liu and E.M. Sparrow, '*Fully Developed Flow and Heat Transfer in Ducts Having Streamwise-Periodic Variations of Cross-Sectional Area*', Journal of Heat Transfer, Transactions of the ASME, Vol. 99, N°2, pp. 180 – 186, 1977.

[19] B.N. Prasad and J.S. Saini, '*Effect of Artificial Roughness on Heat Transfer and Friction Factor in a Solar Air Heater*', Solar Energy, Vol. 41, N°6, pp. 555 - 560, 1988.

[20] M.M. Sahu and J.L. Bhagoria, '*Augmentation of Heat Transfer Coefficient by Using 90 Broken Transverse Ribs on Absorber Plate of Solar Air Heater*', Renewable Energy, Vol. 30, N°13, pp. 2057 -2073, 2005.

[21] R.P. Saini and J.S. Saini, '*Heat Transfer and Friction Factor Correlations for Artificially Roughened Ducts with Expanded Metal Mesh as Roughened Element*', International Journal of Heat and Mass Transfer, Vol. 40, N°4, pp. 973 – 986, 1997.

[22] S.K. Saini and R.P. Saini, '*Development of Correlations for Nusselt Number and Friction Factor for Solar Air Heater with Roughened Duct Having Arc-Shaped Wire as Artificial Roughness*', Solar Energy, Vol. 82, N°12, pp. 1118 – 1130, 2008.